

Solving the relativistic magnetohydrodynamics equations with ADER discontinuous Galerkin methods, a posteriori subcell limiting and adaptive mesh refinement

O. Zanotti^{1*}, F. Fambri¹, M. Dumbser¹

¹Laboratory of Applied Mathematics, University of Trento, Via Mesiano 77, I-38123 Trento, Italy

ABSTRACT

We present a new numerical tool for solving the special relativistic ideal MHD equations that is based on the combination of the following three key features: (i) a one-step ADER discontinuous Galerkin (DG) scheme that allows for an *arbitrary* order of accuracy in both space and time, (ii) an *a posteriori* subcell finite volume limiter that is activated to avoid spurious oscillations at discontinuities without destroying the natural subcell resolution capabilities of the DG finite element framework and finally (iii) a space-time adaptive mesh refinement (AMR) framework with time-accurate local time-stepping.

The divergence-free character of the magnetic field is instead taken into account through the so-called "divergence-cleaning" approach. The convergence of the new scheme is verified up to 5th order in space and time and the results for a sample of significant numerical tests including shock tube problems, the RMHD rotor problem and the Orszag-Tang vortex system are shown. We also consider a simple case of the relativistic Kelvin–Helmholtz instability with a magnetic field, emphasizing the potential of the new method for studying turbulent RMHD flows. We discuss the advantages of our new approach when the equations of relativistic MHD need to be solved with high accuracy within various astrophysical systems.

Key words: magnetohydrodynamics, special relativity, ADER discontinuous Galerkin, a posteriori subcell limiter, adaptive mesh refinement, local time stepping

1 INTRODUCTION

Special relativistic magnetohydrodynamics (RMHD) is supposed to provide a sufficiently accurate description of the dynamics of those astrophysical plasma that move close to the speed of light and which are subject to electromagnetic forces dominating over gravitational forces. This is the case of high energy astrophysical phenomena like extragalactic jets (Begelman et al. 1984), gamma-ray bursts (Kouveliotou et al. 1993) and magnetospheres of neutron stars (Michel 1991). In all these physical systems, in fact, leaving aside the problem of the origin of relativistic jets, which clearly involves the role of the accretion disc and of the corresponding central compact object, general relativistic effects can be fairly neglected. The degree of complexity related to magnetohydrodynamics can of course vary notably. For example, as a first approximation we can neglect dissipation due to resistivity, or we can consider the fluid as a single-component one, although we know for sure that both magnetic reconnection and multi-fluids effects can become important under specific physical conditions.

The numerical solution of the special relativistic magnetohydrodynamics equations has been particularly fostered by the introduction of Godunov methods based on Riemann solvers, which had already been successfully applied to relativistic hydrodynamics. This was the approach followed in the pioneering works by Komissarov (1999) and Balsara (2001a), who implemented for the first time second order Total Variation Diminishing (TVD) schemes with a specific interest towards astrophysical applications. Since then, relativistic magnetohydrodynamics has developed along different directions with impressive results. From one side several approximate Riemann solvers have been introduced (Mignone & Bodo 2006; Honkila

* E-mail: olindo.zanotti@unitn.it

& Janhunen 2007; Mignone et al. 2009; Kim & Balsara 2014). From another side, relativistic magnetohydrodynamics has been extended to the general relativistic regime (Duez et al. 2005; Baumgarte & Shapiro 2003; Antón et al. 2006; Del Zanna et al. 2007; Giacomazzo & Rezzolla 2007), and it is currently used to study a variety of high energy physical processes. An additional direction of research has been represented by the inclusion of dissipative effects, namely non-ideal resistive magnetohydrodynamics, with encouraging results (Komissarov 2007; Palenzuela et al. 2009; Dumbser & Zanotti 2009; Zenitani et al. 2010; Takamoto & Inoue 2011; Bucciantini & Del Zanna 2013). Moreover, high order numerical schemes have also been pursued (Del Zanna et al. 2003; Anderson et al. 2006), while simulations of multi-fluids in RMHD are emerging as a new frontier (Zenitani et al. 2009; Barkov et al. 2014). Finally, Adaptive Mesh Refinement (AMR) within RMHD codes has been also considered (Balsara 2001b; Neilsen et al. 2006; Etienne et al. 2010; Mignone et al. 2012; Keppens et al. 2012; Zanotti & Dumbser 2015) and it is an active field of research. In most of the approaches mentioned so far the evolution in time is performed through the method of lines, resulting in multistep Runge–Kutta schemes, either explicit or implicit. A valuable alternative is provided by ADER schemes, which were introduced by Titarev & Toro (2005); Toro & Titarev (2002) and became popular after the modern reformulation by Dumbser et al. (2008); Dumbser et al. (2008); Balsara et al. (2013). In a nutshell, ADER schemes are high order numerical schemes with a single step for the time update and they have been already applied to the equations of relativistic MHD, both in the ideal case (Dumbser et al. 2008; Zanotti & Dumbser 2015) and in the resistive case (Dumbser & Zanotti 2009). Another common choice that is typically adopted in the majority of modern RMHD codes is that of using finite difference or finite volume conservative schemes. Although rather successful, these schemes require larger and larger stencils when the order of accuracy is increased, a fact that can give rise to substantial overhead when they are parallelized. Discontinuous Galerkin (DG) schemes (Cockburn & Shu 1989; Cockburn et al. 1989, 1990; Cockburn & Shu 1998), on the contrary, do not need any spatial reconstruction and they allow for an arbitrary order of accuracy. DG schemes are still relatively unknown in high energy astrophysics, and only a few investigations have been performed so far in the relativistic regime (Zumbusch 2009; Radice & Rezzolla 2011; Zanotti & Dumbser 2011). Unfortunately, DG schemes suffer from a serious problem, which has negatively affected their popularity. Namely, since they are linear in the sense of Godunov’s theorem, they produce oscillations as soon as a discontinuity appears in the solution, even though they exploit the conservative formulation of the equations and even though Riemann solvers are used for the computation of the fluxes. The procedures that have been adopted to overcome this difficulty can be roughly divided in two classes. From one side, it is possible to introduce additional numerical dissipation, either in the form of artificial viscosity (R.Hartmann & P.Houston 2002; Persson & Peraire 2006; Cesenek et al. 2013), or by means of filtering (Radice & Rezzolla 2011). From another side, it is possible to isolate the so-called *troubled cells*, namely those affected by spurious oscillations, and adopt for them some sort of nonlinear finite-volume-type slope-limiting procedure (Cockburn & Shu 1998; Qiu & Shu 2005; J.Qiu & C-W.Shu 2004; Balsara et al. 2007; J.Zhu et al. 2008; J.Zhu & Qiu 2013; H.Luo et al. 2007; L.Krivodonova 2007), either based on nonlinear WENO/HWENO reconstruction or by applying a TVB limiter to the higher order moments of the discrete solution. The drawback of this strategy is that in most cases the subcell resolution properties of the DG scheme are immediately lost.

Very recently, a promising alternative has been proposed by Dumbser et al. (2014), which is based on a previous idea of Clain et al. (2011) and Diot et al. (2012) called MOOD (multi-dimensional optimal order detection), and which adopts an *a posteriori* approach to the problem of limiting of high order schemes in the finite volume framework. In a few words, the novel *a posteriori* DG limiter method of Dumbser et al. (2014) consists of (i) computing the solution by means of an *unlimited* ADER-DG scheme, (ii) detecting *a posteriori* the troubled cells by applying a simple discrete maximum principle (DMP) and positivity of density and pressure on the discrete solution, (iii) creating a local sub-grid within these troubled DG cells, and (iv) *recomputing* the discrete solution at the sub-grid level via a more robust Total Variation Diminishing (TVD) or Weighted Essentially Non Oscillatory (WENO) finite volume scheme. The final non-oscillatory DG solution on the main grid is then recovered from the subcell averages by means of a finite-volume reconstruction operator that acts on the cell averages of the subgrid. In the present paper we apply this idea for the first time to solve the RMHD equations in combination with space-time adaptive mesh refinement and time-accurate local time stepping, extending a similar work proposed for classical fluid dynamics by Zanotti et al. (2014). For alternative work on DG subcell limiters see also (Casoni et al. 2013; Sonntag & Munz 2014; Fechter & Munz 2015).

The plan of the paper is the following. In Section 2 we report the RMHD equations and the basic physical assumptions, while Section 3 is devoted to the presentation of the numerical method, which is validated in Section 4. Section 5 contains a first simple analysis of the turbulence induced by the Kelvin–Helmholtz instability, while in Section 6 we conclude the work. We have considered a flat spacetime in pseudo-Cartesian coordinates, namely the metric $\eta_{\mu\nu} = \text{diag}(-1, 1, 1, 1)$, where Greek letters run from 0 to 3 and Latin letters i, j, k, \dots run from 1 to 3. The speed of light is set to $c = 1$ and we make use of the Lorentz-Heaviside notation for the electromagnetic quantities, such that all $\sqrt{4\pi}$ factors disappear. Finally, we use Einstein summation convention over repeated indices.

2 MATHEMATICAL FORMULATION AND PHYSICAL ASSUMPTIONS

The energy-momentum tensor of a single-component plasma with infinite conductivity is given by (Anile 1990)

$$T^{\mu\nu} = (\rho h + b^2)u^\mu u^\nu + (p + b^2/2)\eta^{\mu\nu} - b^\mu b^\nu, \quad (1)$$

where u^μ is the four velocity of the fluid, b^μ is the four vector magnetic field, $b^2 = b_\mu b^\mu$, while h , ρ and p are the specific enthalpy, the rest mass density and the thermal pressure, each of them measured in the co-moving frame of the fluid. The metric of the spacetime is the Minkowski one, namely $\eta^{\mu\nu} = \eta_{\mu\nu} = \text{diag}(-1, 1, 1, 1)$. We recall that in ideal MHD the electric field in the comoving frame of the fluid vanishes. If we instead select a static laboratory observer defined by the four-velocity vector $n^\mu = (-1, 0, 0, 0)$, then the electric field E^μ and B^μ measured in such a frame are related to the electromagnetic tensor $F^{\mu\nu}$, and to its dual $F^{*\mu\nu}$, by

$$F^{\mu\nu} = n^\mu E^\nu - E^\mu n^\nu + \epsilon^{\mu\nu\lambda\kappa} B_\lambda n_\kappa \quad (2)$$

$$F^{*\mu\nu} = n^\mu B^\nu - B^\mu n^\nu - \epsilon^{\mu\nu\lambda\kappa} E_\lambda n_\kappa, \quad (3)$$

where $\epsilon^{\mu\nu\lambda\kappa}$ is the completely antisymmetric spacetime Levi-Civita tensor, with the convention that $\epsilon^{0123} = 1$. Note that the four vectors of the electric and of the magnetic field are purely spatial, i.e. $E^0 = B^0 = 0$, $E^i = E_i$, $B^i = B_i$. Moreover, the fluid four velocity u^μ and the standard three velocity in the laboratory frame are related as $v^i = u^i/W$, where $W = (1 - v^2)^{-1/2}$ is the Lorentz factor of the fluid. We stress that the electric field does not need to be evolved in time through the Maxwell equations, since within the ideal MHD assumption it can always be computed a posteriori as $\vec{E} = -\vec{v} \times \vec{B}$. In the rest of the paper we also assume that the fluid obeys the ideal gas equation of state, namely

$$p = \rho\epsilon(\gamma - 1), \quad (4)$$

where ϵ is the specific internal energy, which is a function of the temperature only, and γ is the adiabatic index. The equations of ideal RMHD, which in covariant form are

$$\nabla_\alpha(\rho u^\alpha) = 0, \quad (5)$$

$$\nabla_\alpha T^{\alpha\beta} = 0, \quad (6)$$

$$\nabla_\alpha F^{*\alpha\beta} = 0, \quad (7)$$

for numerical purposes are better expressed in conservative form as (Komissarov 1999; Balsara 2001a)

$$\partial_t \mathbf{u} + \partial_i \mathbf{f}^i = 0, \quad (8)$$

where the conserved variables and the corresponding fluxes in the i direction are given by¹

$$\mathbf{u} = \begin{bmatrix} D \\ S_j \\ U \\ B^j \end{bmatrix}, \quad \mathbf{f}^i = \begin{bmatrix} v^i D \\ W_j^i \\ S^i \\ \epsilon^{jik} E^k \end{bmatrix}. \quad (9)$$

The conserved variables (D, S_j, U, B^j) are related to the rest-mass density ρ , to the thermal pressure p , to the fluid velocity v_i and to the magnetic field B^i by

$$D = \rho W, \quad (10)$$

$$S_i = \rho h W^2 v_i + \epsilon_{ijk} E_j B_k, \quad (11)$$

$$U = \rho h W^2 - p + \frac{1}{2}(E^2 + B^2), \quad (12)$$

where ϵ_{ijk} is the spatial Levi-Civita tensor and δ_{ij} is the Kronecker symbol. The spatial tensor W_j^i in (9), representing the momentum flux density, is

$$W_{ij} \equiv \rho h W^2 v_i v_j - E_i E_j - B_i B_j + \left[p + \frac{1}{2}(E^2 + B^2) \right] \delta_{ij}, \quad (13)$$

where δ_{ij} is the Kronecker delta. Eqs. (7) above include the divergence free condition $\vec{\nabla} \cdot \vec{B} = 0$. Although the Maxwell equations guarantee that such a constraint is mathematically fulfilled for all times if it is satisfied in the initial conditions, from a numerical point of view specific actions must be taken in order to preserve the divergence-free property of the magnetic field during the evolution of the system. Several strategies have been proposed over the years to solve this problem [see Toth (2000) for a review]. In this paper we have adopted the so called *divergence-cleaning approach* presented in Dedner et al.

¹ Although formally written in conservative form, the evolution of the magnetic field is based on Stokes' theorem rather than on Gauss' theorem. See Londrillo & Del Zanna (2000) for a careful discussion about these aspects.

(2002), which amounts to augmenting the system (8) with an additional equation for a scalar field Φ , in order to propagate away the deviations from $\vec{\nabla} \cdot \vec{B} = 0$. Hence, we must solve

$$\partial_t \Phi + \partial_i B^i = -\kappa \Phi, \quad (14)$$

while the fluxes for the evolution of the magnetic field are also modified, namely $\mathbf{f}^i(B^j) \rightarrow \epsilon^{ijk} E^k + \Phi \delta^{ij}$. The damping coefficient κ in Eq. (14) drives the solution towards $\vec{\nabla} \cdot \vec{B} = 0$ over a timescale $1/\kappa$. In our calculations we have typically used $\kappa \in [1; 10]$. More details about this approach can be found in Komissarov (2007), Palenzuela et al. (2009), Dionysopoulou et al. (2013).

As well known, in the relativistic framework the conversion from the conserved variables (D, S_i, U, B_i) to the primitive variables (p, ρ, v_i, B_i) , which are needed for the computation of the fluxes, is not analytic, and a numerical root-finding approach is therefore needed. In our numerical code we adopted the third method reported in Sect. 3.2 of Del Zanna et al. (2007). A full account about alternative methods to invert the system (10)–(12) was given in Noble et al. (2006). Additional information about the mathematical properties of the RMHD equations can be found in Balsara & Spicer (1999); Komissarov (1999); Antón et al. (2006); Del Zanna et al. (2007); Antón et al. (2010). The latter, in particular, contains a detailed discussion about the renormalization of the eigenvectors of the associated Jacobian.

3 NUMERICAL METHOD

The numerical scheme that we adopt results from the combination of a few different steps, which in principle could be used separately. Here we provide a brief but self-consistent presentation of the scheme, while addressing to Dumbser et al. (2014) and to Zanotti et al. (2014) for additional discussion.

3.1 Basic mathematical definitions

We use spatial Cartesian coordinates over a domain Ω which is composed by elements T_i as

$$\Omega = \bigcup_{i=1}^{N_E} T_i, \quad (15)$$

where the index i ranges from 1 to the total number of elements N_E . At the generic time t^n , the numerical solution of Eq. (8) is represented within each cell T_i by polynomials of maximum degree $N \geq 0$, namely

$$\mathbf{u}_h(\mathbf{x}, t^n) = \sum_{l=0}^N \Phi_l(\mathbf{x}) \hat{\mathbf{u}}_l^n = \Phi_l(\mathbf{x}) \hat{\mathbf{u}}_l^n \quad \mathbf{x} \in T_i, \quad (16)$$

where \mathbf{u}_h is referred to as the *discrete representation* of the solution, while the coefficients $\hat{\mathbf{u}}_l^n$ are the *degrees of freedom*.² In one spatial dimension, the basis functions $\Phi_l(x)$ are given by the Lagrange interpolation polynomials, all of degree N , which pass through the $(N+1)$ Gauss-Legendre quadrature points (Solin 2006). The resulting basis is therefore a nodal basis, with the property that $\Phi_l(x_k) = \delta_{lk}$, where x_k are the coordinates of the Gauss-Legendre nodal points. In multiple space dimensions, the basis functions $\Phi_l(\mathbf{x})$ are the dyadic products of the one-dimensional basis.

3.2 The Discontinuous Galerkin scheme

The system of equations (8) is in conservative form and, therefore, numerical schemes derived from it are guaranteed to converge to the weak solution (Lax & Wendroff 1960), even if this contains a discontinuity. The vast majority of numerical schemes for the solution of the RMHD equations use either conservative finite difference or finite volume schemes, which incorporate in a natural way Riemann solvers, thus assuring the upwind property of the method. An effective alternative to these approaches is represented by Discontinuous Galerkin methods (Cockburn & Shu 1991, 1989; Cockburn et al. 1990; Cockburn & Shu 1998), which still exploit the conservative form of the equations and the usage of Riemann solvers, but which evolve in time the degrees of freedom with respect to the chosen basis, rather than the point values or the cell averages of the solution.

To illustrate the method, we first multiply the governing equations (8) by a test function $\Phi_k \in \mathcal{U}_h$, identical to the spatial

² Here we slightly abuse of the Einstein summation convention, which is adopted even if the mute indices over which the summation is performed do not refer to co-variant and contra-variant vectors.

basis functions of Eq. (16). After that, we integrate over the space-time control volume $T_i \times [t^n; t^{n+1}]$. If we integrate by parts in space the flux divergence term, we obtain

$$\int_{t^n}^{t^{n+1}} \int_{T_i} \Phi_k \frac{\partial \mathbf{u}_h}{\partial t} d\mathbf{x} dt + \int_{t^n}^{t^{n+1}} \int_{\partial T_i} \Phi_k \mathbf{f}(\mathbf{u}_h) \cdot \mathbf{n} dS dt - \int_{t^n}^{t^{n+1}} \int_{T_i} \nabla \Phi_k \cdot \mathbf{f}(\mathbf{u}_h) d\mathbf{x} dt = 0, \quad (17)$$

where \mathbf{n} is the outward pointing unit normal vector on the surface ∂T_i of element T_i . The second term of Eq. (17) contains a surface integration, which is conveniently performed through the solution of a Riemann problem at the element boundary, like in traditional conservative finite volume schemes. This guarantees that the final method is upwind. The time integration of Eq. (17) can be performed through Runge–Kutta schemes, leading to RKDG schemes (Cockburn & Shu 1991, 1989; Cockburn et al. 1989, 1990; Cockburn & Shu 1998; H.Zhu & J.Qiu 2013) but it can also be obtained through the ADER philosophy, see (Dumbser & Munz 2006; Qiu et al. 2005). More precisely, we want to devise a one-step time integration scheme for (17), while preserving high order of accuracy both in space and in time. This can be done, provided an approximate *predictor* state \mathbf{q}_h is available at any intermediate time between t^n and t^{n+1} and with the same spatial accuracy of the initial DG polynomial. We have denoted this spacetime predictor solution \mathbf{q}_h with a separate symbol, to distinguish it from the discrete solution of the DG scheme \mathbf{u}_h . After inserting \mathbf{u}_h , as given by (16), in the first term of (17) and by using the spacetime predictor \mathbf{q}_h in the other terms, we find the following one-step ADER discontinuous Galerkin scheme:

$$\left(\int_{T_i} \Phi_k \Phi_l d\mathbf{x} \right) (\hat{\mathbf{u}}_l^{n+1} - \hat{\mathbf{u}}_l^n) + \int_{t^n}^{t^{n+1}} \int_{\partial T_i} \Phi_k \mathcal{G}(\mathbf{q}_h^-, \mathbf{q}_h^+) \cdot \mathbf{n} dS dt - \int_{t^n}^{t^{n+1}} \int_{T_i} \nabla \Phi_k \cdot \mathbf{f}(\mathbf{q}_h) d\mathbf{x} dt = 0. \quad (18)$$

In the equation above \mathcal{G} is a numerical flux function, which in practice is given by a Riemann solver, while \mathbf{q}_h^- and \mathbf{q}_h^+ are the corresponding left and right states of the spacetime predictor solution that is typical of ADER schemes. This will allow us to compute the spacetime integrals of the second and of the third terms of Eq. (18) to the desired order of accuracy. The strategy for obtaining the predictor \mathbf{q}_h from the DG polynomials \mathbf{u}_h is explained in Sect. 3.3. Concerning the choice of the Riemann solver, in this paper we have used the simple Rusanov flux and the HLL solver (Toro 1999).

3.3 The spacetime discontinuous Galerkin predictor

In the original ADER approach by Titarev & Toro (2002) and Titarev & Toro (2005), the time evolution \mathbf{q}_h of the data \mathbf{u}_h available at time t^n is obtained by means of the so-called Cauchy-Kowalevski procedure, which implies a Taylor expansion in time, and a subsequent replacement of time derivatives with spatial derivatives through the governing system of PDEs. As simple as it is in principle, this approach becomes prohibitively complex for highly non-linear systems of equations. It has been successfully implemented for the classical Euler equations (Dumbser et al. 2007) but it has never been extended to the relativistic regime. In the modern ADER version proposed by Dumbser et al. (2008), the time evolution is instead performed through a spacetime discontinuous Galerkin predictor, which operates locally for each cell. To illustrate the method, we first transform the PDE system of Eq. (8) into a space-time reference coordinate system (ξ, η, ζ, τ) . Hence, the space-time control volume $\mathcal{C}_{ijkn} = [x_{i-\frac{1}{2}}; x_{i+\frac{1}{2}}] \times [y_{j-\frac{1}{2}}; y_{j+\frac{1}{2}}] \times [z_{k-\frac{1}{2}}; z_{k+\frac{1}{2}}] \times [t^n; t^{n+1}]$ is mapped into the space-time reference element $T_E \times [0; 1]$ as

$$x = x_{i-\frac{1}{2}} + \xi \Delta x_i, \quad y = y_{j-\frac{1}{2}} + \eta \Delta y_j, \quad z = z_{k-\frac{1}{2}} + \zeta \Delta z_k, \quad t = t^n + \tau \Delta t, \quad (19)$$

where $T_E = [0; 1]^d$ denotes the spatial reference element in d spatial dimensions. In these reference coordinates, Eq. (8) rephrases into

$$\frac{\partial \mathbf{u}}{\partial \tau} + \nabla_\xi \cdot \mathbf{f}^*(\mathbf{u}) = 0, \quad (20)$$

where

$$\mathbf{f}^* := \Delta t (\partial \xi / \partial \mathbf{x})^T \cdot \mathbf{f}(\mathbf{u}), \quad (21)$$

with $\boldsymbol{\xi} = (\xi, \eta, \zeta)$ and $\nabla_\xi = \partial \boldsymbol{\xi} / \partial \mathbf{x} \cdot \nabla$. We now multiply (20) by a space-time test function $\theta_k = \theta_k(\boldsymbol{\xi}, \tau)$ and integrate over the space-time reference control volume $T_E \times [0; 1]$, to obtain

$$\int_0^1 \int_{T_E} \theta_k \frac{\partial \mathbf{u}}{\partial \tau} d\boldsymbol{\xi} d\tau + \int_0^1 \int_{T_E} \theta_k \nabla_\xi \cdot \mathbf{f}^*(\mathbf{u}) d\boldsymbol{\xi} d\tau = 0. \quad (22)$$

The *discrete spacetime solution* of equation (22) is the \mathbf{q}_h that we have mentioned above. In analogy to Eq. (16), we expand it as

$$\mathbf{q}_h = \mathbf{q}_h(\boldsymbol{\xi}, \tau) = \theta_l \hat{\mathbf{q}}_l. \quad (23)$$

Something similar is done for the fluxes, which are represented as

$$\mathbf{f}_h^* = \mathbf{f}_h^*(\boldsymbol{\xi}, \tau) = \theta_l \hat{\mathbf{f}}_l^*. \quad (24)$$

Both the space-time test function θ_k in Eq. (22) and the basis functions θ_l are chosen as dyadic products of Lagrange interpolation polynomials passing through the Gauss-Legendre quadrature points. As a result, the degrees of freedom for the fluxes can be computed as the point-wise evaluation of the physical fluxes, i.e.

$$\hat{\mathbf{f}}_l^* = \mathbf{f}^*(\hat{\mathbf{q}}_l). \quad (25)$$

Since the time evolution of the discrete solution \mathbf{q}_h is now hidden in the basis functions, we can integrate the first term by parts in time in (22), which allows us to introduce the DG solution $\mathbf{u}_h(\mathbf{x}, t^n)$ as initial condition at time t^n in a weak form. We thus obtain

$$\int_{T_E} \theta_k(\boldsymbol{\xi}, 1) \mathbf{q}_h d\boldsymbol{\xi} - \int_{T_E} \theta_k(\boldsymbol{\xi}, 0) \mathbf{u}_h d\boldsymbol{\xi} - \int_0^1 \int_{T_E} \frac{\partial \theta_k}{\partial \tau} \mathbf{q}_h d\boldsymbol{\xi} d\tau + \int_0^1 \int_{T_E} \theta_k \nabla_{\boldsymbol{\xi}} \cdot \mathbf{f}_h^* d\boldsymbol{\xi} d\tau = 0. \quad (26)$$

Inserting (23) and (24) into Eq. (26) provides (Dumbser et al. 2008; Hidalgo & Dumbser 2011; Dumbser & Zanotti 2009)

$$\left(\int_{T_E} \theta_k(\boldsymbol{\xi}, 1) \theta_l(\boldsymbol{\xi}, 1) d\boldsymbol{\xi} - \int_0^1 \int_{T_E} \frac{\partial \theta_k}{\partial \tau} \theta_l d\boldsymbol{\xi} d\tau \right) \hat{\mathbf{q}}_l = \left(\int_{T_E} \theta_k(\boldsymbol{\xi}, 0) \Phi_l d\boldsymbol{\xi} \right) \hat{\mathbf{u}}_l^n - \left(\int_0^1 \int_{T_E} \theta_k \nabla_{\boldsymbol{\xi}} \theta_l d\boldsymbol{\xi} d\tau \right) \mathbf{f}^*(\hat{\mathbf{q}}_l), \quad (27)$$

which is a nonlinear system to be solved in the unknown expansion coefficients $\hat{\mathbf{q}}_l$. A few comments should be given at this stage. The first one is that, being local in space, the spacetime discontinuous Galerkin predictor does not require the solution of any Riemann problem, which is instead invoked in the global scheme (18). The second comment is that the discontinuous Galerkin predictor just described can be used also in combination with more traditional finite volume schemes, which has been done for the RMHD equations for instance in Zanotti & Dumbser (2015). The third comment is that this approach, unlike the original ADER approach, remains valid even in the presence of stiff source terms, as it has been done for various physical systems by Dumbser & Zanotti (2009); Hidalgo & Dumbser (2011); Zanotti et al. (2011); Dumbser et al. (2012). Finally, we emphasize that for DG schemes the timestep must be restricted as (Krivodonova & R.Qin 2013)

$$\Delta t < \frac{1}{d} \frac{1}{(2N+1)} \frac{h}{|\lambda_{\max}|}, \quad (28)$$

where h and $|\lambda_{\max}|$ are a characteristic mesh size and the maximum signal velocity, respectively.

3.4 An *a posteriori* subcell limiter

Should we implement the ADER-DG scheme as it is described in the two previous Sections, we would obtain a numerical scheme capable of resolving smooth solutions with an order of accuracy equal to $N+1$, where N is the degree of the chosen polynomials, but totally inadequate for discontinuous solutions, for which the Gibbs phenomenon would quickly lead to spurious oscillations and even to a breakdown of the scheme. A novel idea for an *a posteriori* limiter has been recently proposed by Dumbser et al. (2014) and it works as follows.

- The *unlimited* ADER-DG scheme (18) is first used to evolve the solution from time t^n to t^{n+1} , producing a so-called candidate solution $\mathbf{u}_h^*(\mathbf{x}, t^{n+1})$ inside each cell.

- The candidate solution $\mathbf{u}_h^*(\mathbf{x}, t^{n+1})$ is then checked against two different criteria to verify its validity, namely

- Physical admissibility detection*: if the conversion from conservative to primitive variables fails, or if either the pressure or the rest mass density drops below a threshold value, or if we encounter superluminal velocities, then the cell is flagged as *troubled*.

- Numerical admissibility detection*: if the polynomial representing the candidate solution does not lie between the minimum and the maximum of the polynomials representing the solution at the previous time step in the set \mathcal{V}_i , then the cell is flagged as *troubled*. The set \mathcal{V}_i contains the cell T_i and all its Voronoi neighbor cells that share a common node with T_i . This second detection criterion is specifically designed to remove spurious Gibbs oscillations from the solution.

- As soon as a cell is flagged as troubled at the future time t^{n+1} , it generates a local sub-grid formed by $N_s = 2N+1$ cells per space dimension, each of which is assigned a subcell average $\mathbf{v}_h(\mathbf{x}, t^n)$ by means of a L_2 projection obtained from the DG polynomial at the *previous time level* t^n , i.e.

$$v_{i,j}^n = \frac{1}{|S_{i,j}|} \int_{S_{i,j}} \mathbf{u}_h(\mathbf{x}, t^n) d\mathbf{x} = \frac{1}{|S_{i,j}|} \int_{S_{i,j}} \hat{\mathbf{u}}_l^n \phi_l(\mathbf{x}) d\mathbf{x}, \quad \forall S_{i,j} \in \mathcal{S}_i, \quad (29)$$

where $\mathcal{S}_i = \bigcup_j S_{i,j}$ is the set of the sub-grid cells. In this way the high accuracy of the DG polynomial is transferred to the subgrid level *before* the spurious oscillations arise. We have chosen $N_s = 2N+1$ in order to guarantee that the maximum

timestep of the ADER-DG scheme on the main grid (c.f. Eq. (28)) matches the maximum possible time step of the ADER finite volume scheme on the sub-grid.

- The alternative data representation, provided by Eq. (29), is now used as initial condition to evolve the discrete solution with a more robust finite volume scheme on the sub-grid. This is done by resorting to either an ADER-WENO finite volume scheme, or to an even more robust second order TVD shock capturing scheme. For details about the implementation of WENO within our ADER framework we refer to Dumbser et al. (2013); Zanotti & Dumbser (2015). In practice, on the sub-grid a new evolution from time t^n to t^{n+1} is performed combining a third order WENO finite volume scheme with the spacetime discontinuous Galerkin predictor described in Sect. 3.3. Only for particularly challenging problems we sacrifice WENO in favor of a simpler second order TVD scheme. We emphasize that both the DG scheme on the main grid as well as the WENO finite volume scheme on the sub-grid are *one-step* ADER schemes.

- The last step requires that the new solution at time t^{n+1} over the sub-grid is projected back to the main grid. This is done imposing that

$$\int_{S_{i,j}} \mathbf{u}_h(\mathbf{x}, t^{n+1}) d\mathbf{x} = \int_{S_{i,j}} \mathbf{v}_h(\mathbf{x}, t^{n+1}) d\mathbf{x}, \quad \forall S_{i,j} \in \mathcal{S}_i. \quad (30)$$

which is a standard reconstruction problem in high order finite volume methods (Barth & Frederickson 1990; Titarev & Toro 2004; Titarev & Toro 2005; Dumbser et al. 2013) and spectral finite volume schemes (Wang et al. 2004; Liu et al. 2006).

In all the numerical simulations described in Sect. 4, the DG scheme over the main grid has been implemented with $N \in [2; 5]$, hence up to the sixth order of accuracy both in space and in time, while the WENO scheme on the sub-grid is always at the third order. Moreover, in the Figs. 1 and 4 below we have represented in blue the unlimited cells, namely those that have been successfully evolved through the standard ADER-DG scheme, while we have represented in red the troubled cells, which required the activation of the subcell limiter.

3.5 Adaptive Mesh Refinement

The whole scheme described so far can be implemented over adaptively refined meshes (AMR), together with time-accurate local time-stepping (LTS). In Dumbser et al. (2013), Zanotti et al. (2014) and Zanotti & Dumbser (2015) we have already described all details of our AMR strategy, hence, in the following we recall the most important aspects only.

Our AMR approach can be referred to as a "cell-by-cell" refinement (Khokhlov 1998), according to which every cell T_i is individually refined with no creation of grid patches. As customary, the refinement criterion involves up to the second order derivative of a suitable *indicator function* Φ , in terms of which a suitable refinement function is build (Lhner 1987),

$$\chi_m(\Phi) = \sqrt{\frac{\sum_{k,l} (\partial^2 \Phi / \partial x_k \partial x_l)^2}{\sum_{k,l} \left[\left(|\partial \Phi / \partial x_k|_{i+1} + |\partial \Phi / \partial x_k|_i \right) / \Delta x_l + \epsilon \left| \frac{\partial^2}{\partial x_k \partial x_l} |\Phi| \right|^2 \right]}}. \quad (31)$$

The refinement function χ_m is checked for each cell T_i , and if $\chi_i > \chi_{\text{ref}}$, the cell is refined, while it is recoarsened if $\chi_i < \chi_{\text{rec}}$. In most of our simulations, except for Sect. 4.1 where we have used $\Phi = B_y$, the indicator function has been assumed to be the relativistic mass density, i.e. $\Phi = D = W\rho$. The implementation of the AMR infrastructure is based on the following general rules:

- A maximum level of refinement ℓ_{max} is chosen, such that $0 \leq \ell \leq \ell_{\text{max}}$, where ℓ indicates the actual refinement level.
- When a *mother cell* T_i is refined, it generates τ^d *children cells*, where d is the spatial dimension, while τ is the refinement factor, typically chosen between 2 and 4.
- Each cell T_i , at any level of refinement, is given a specific *status*, denoted by σ for convenience, with the following meaning
 - active cell* ($\sigma = 0$), updated through the standard ADER-DG scheme;
 - virtual child cell* ($\sigma = 1$), updated according to standard L_2 projection of the high order polynomial of the mother cell at the $(\ell - 1)$ -th level;
 - virtual mother cell* ($\sigma = -1$), updated by recursively averaging over all children cells from higher refinement levels.

A virtual child cell has always an active mother cell, while a virtual mother cell has children with status $\sigma \leq 0$.

- Only active cells ($\sigma = 0$) can be refined. Hence, if a virtual cell needs to be refined, it must be first activated.
- The levels of refinement of two cells that are Voronoi neighbors³ of each other can only differ by at most unity. Moreover, every cell has Voronoi neighbors, which can be either active or virtual, at the same level of refinement.

³ The *Voronoi neighbors* \mathcal{V}_i of a cell T_i are cells which share common nodes.

| 2D circularly polarized Alfvén Wave problem — ADER-DG- \mathbb{P}_N + WENO3 SCL | | | | | | | | |
|---|-------|-------------|-------------|------------------|-------------|-------------|------------------|--------|
| | N_x | L_1 error | L_2 error | L_∞ error | L_1 order | L_2 order | L_∞ order | Theor. |
| DG- \mathbb{P}_2 | 30 | 2.9861E-3 | 7.2314E-4 | 4.2388E-4 | — | — | — | 3 |
| | 60 | 2.9229E-4 | 8.0346E-5 | 7.0230E-5 | 3.35 | 3.17 | 2.59 | |
| | 90 | 8.8069E-5 | 2.5059E-5 | 2.3319E-5 | 2.95 | 2.87 | 2.72 | |
| | 120 | 3.6687E-5 | 1.0900E-5 | 1.0948E-5 | 3.04 | 2.89 | 2.63 | |
| DG- \mathbb{P}_3 | 15 | 1.2671E-4 | 2.5939E-5 | 1.1433E-5 | — | — | — | 4 |
| | 20 | 3.1455E-5 | 6.5949E-6 | 2.9456E-6 | 4.48 | 4.76 | 4.71 | |
| | 25 | 1.1743E-5 | 2.5410E-6 | 1.4527E-6 | 4.41 | 4.27 | 3.17 | |
| | 30 | 5.7046E-6 | 1.2767E-6 | 7.5875E-7 | 3.96 | 3.77 | 3.56 | |
| DG- \mathbb{P}_4 | 10 | 6.6600E-5 | 1.4648E-5 | 7.5420E-6 | — | — | — | 5 |
| | 15 | 7.8640E-6 | 1.9384E-6 | 1.2828E-6 | 5.26 | 4.98 | 4.36 | |
| | 20 | 1.8748E-6 | 4.9562E-7 | 3.6520E-7 | 4.98 | 4.74 | 4.36 | |
| | 25 | 6.1631E-7 | 1.6408E-7 | 1.3283E-7 | 4.98 | 4.95 | 4.53 | |

Table 1. L_1, L_2 and L_∞ errors and convergence rates for the 2D circularly polarized Alfvén wave problem for the ADER-DG- \mathbb{P}_N scheme with subcell limiter and adaptive mesh refinement. Two levels of refinement have been used with a refinement factor $\tau = 3$. The errors have been computed for the variable B^y .

The rules above are quite general, and they would still hold even if a pure finite volume scheme was adopted. In addition to them, a few more instructions are needed when the AMR framework is combined with the presence of the limiter for the DG scheme. Namely,

- The virtual children cells inherit the limiter status of their active mother cell.
- If at least one active child is flagged as troubled, then the (virtual) mother is also flagged as troubled.
- Cells which need the subcell limiting cannot be recoarsened.

A proper description of the AMR-projection and of the AMR-averaging at the sub-grid level involving different levels of refinement can be found in Zanotti et al. (2014).

4 NUMERICAL TESTS

4.1 Convergence test

We have tested the convergence of our new numerical scheme by considering the propagation of a circularly polarized Alfvén wave, for which an analytic solution is known (Komissarov 1997; Del Zanna et al. 2007). Choosing x as the direction of propagation, and η as the amplitude of the wave, the magnetic field is given by

$$B_x = B_0 \tag{32}$$

$$B_y = \eta B_0 \cos[k(x - v_A t)] \tag{33}$$

$$B_z = \eta B_0 \sin[k(x - v_A t)], \tag{34}$$

where B_0 is the uniform magnetic field along x , k is the wave number, while v_A is the Alfvén speed at which the wave propagates (see Del Zanna et al. (2007) for its analytic form). The vector tips of the transverse velocity field describe circles in the yz plane normal to \vec{B}_0 , according to

$$v_y = -v_A B_y / B_0, \quad v_z = -v_A B_z / B_0. \tag{35}$$

We have used $\rho = p = B_0 = \eta = 1$, and since the wave is incompressible, the background values of ρ and p are not affected. The test has been performed in two spatial dimensions, using periodic boundary conditions, over the computational domain $\Omega = [0; 2\pi] \times [0; 2\pi]$. We compare the numerical solution with the analytic one after one period $T = L/v_A = 2\pi/v_A$. The results of this analysis are reported in Tab. 1, which report the L_1, L_2 and L_∞ norms of the error of B^y . The Rusanov flux has been adopted, with $\ell_{\max} = 2$ and a Courant factor CFL = 0.8. We emphasize that, due to the smoothness of the solution, the subcell limiter is never activated. As it is apparent from the table, the nominal order of convergence is essentially confirmed.

4.2 Riemann problems

Once the convergence properties have been verified, we consider a few relevant shock-tube problems to test the new ADER-DG-AMR method. Specifically, we concentrate on two classical Riemann problems for RMHD, already proposed by vanPutten

| Problem | | ρ | $(v_x$ | v_y | $v_z)$ | p | $(B_x$ | B_y | $B_z)$ | t_{final} | γ |
|---|------------|--------|--------|-------|--------|------|--------|-------|--------|--------------------|----------|
| RP1 (Test 1 in Balsara (2001a)) | $x > 0$ | 0.125 | 0.0 | 0.0 | 0.0 | 0.1 | 0.5 | -1.0 | 0.0 | 0.4 | 2.0 |
| | $x \leq 0$ | 1.0 | 0.0 | 0.0 | 0.0 | 1.0 | 0.5 | 1.0 | 0.0 | | |
| RP2 (Test 5 in Balsara (2001a)) | $x > 0$ | 1.0 | -0.45 | -0.2 | 0.2 | 1.0 | 2.0 | -0.7 | 0.5 | 0.55 | 5/3 |
| | $x \leq 0$ | 1.08 | 0.4 | 0.3 | 0.2 | 0.95 | 2.0 | 0.3 | 0.3 | | |

Table 2. Initial conditions for the one-dimensional Riemann problems.

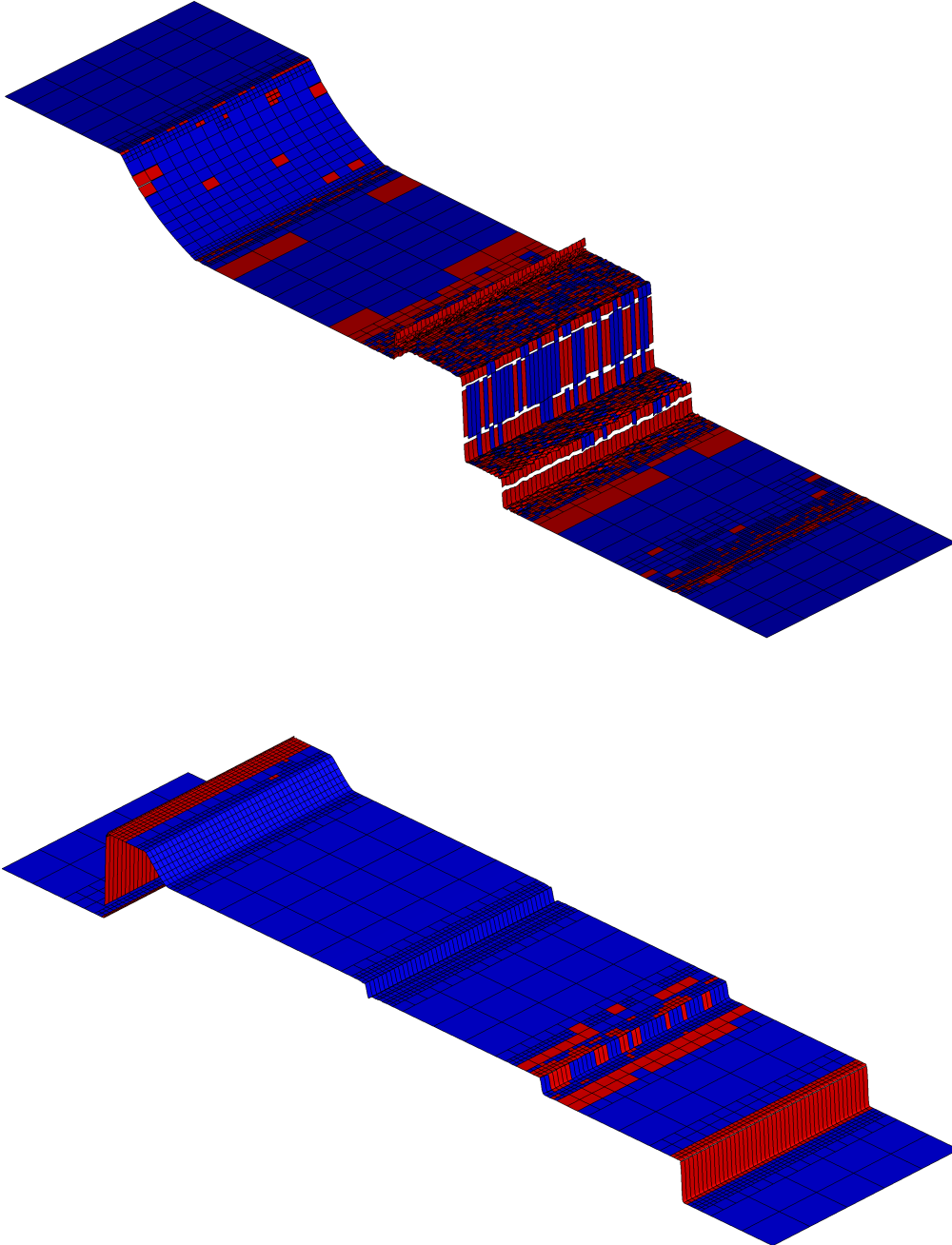


Figure 1. 3D view of the density variable and the corresponding AMR grid. Top panel: RP1 at $t_{\text{final}} = 0.4$ (coarsest grid of 40×5 elements). Bottom panel: RP2 at $t_{\text{final}} = 0.55$ (coarsest grid of 25×5 elements). The limited cells, using the subcell ADER-WENO3 finite volume scheme, are highlighted in red, while unlimited DG- \mathbb{P}_3 cells are highlighted in blue.

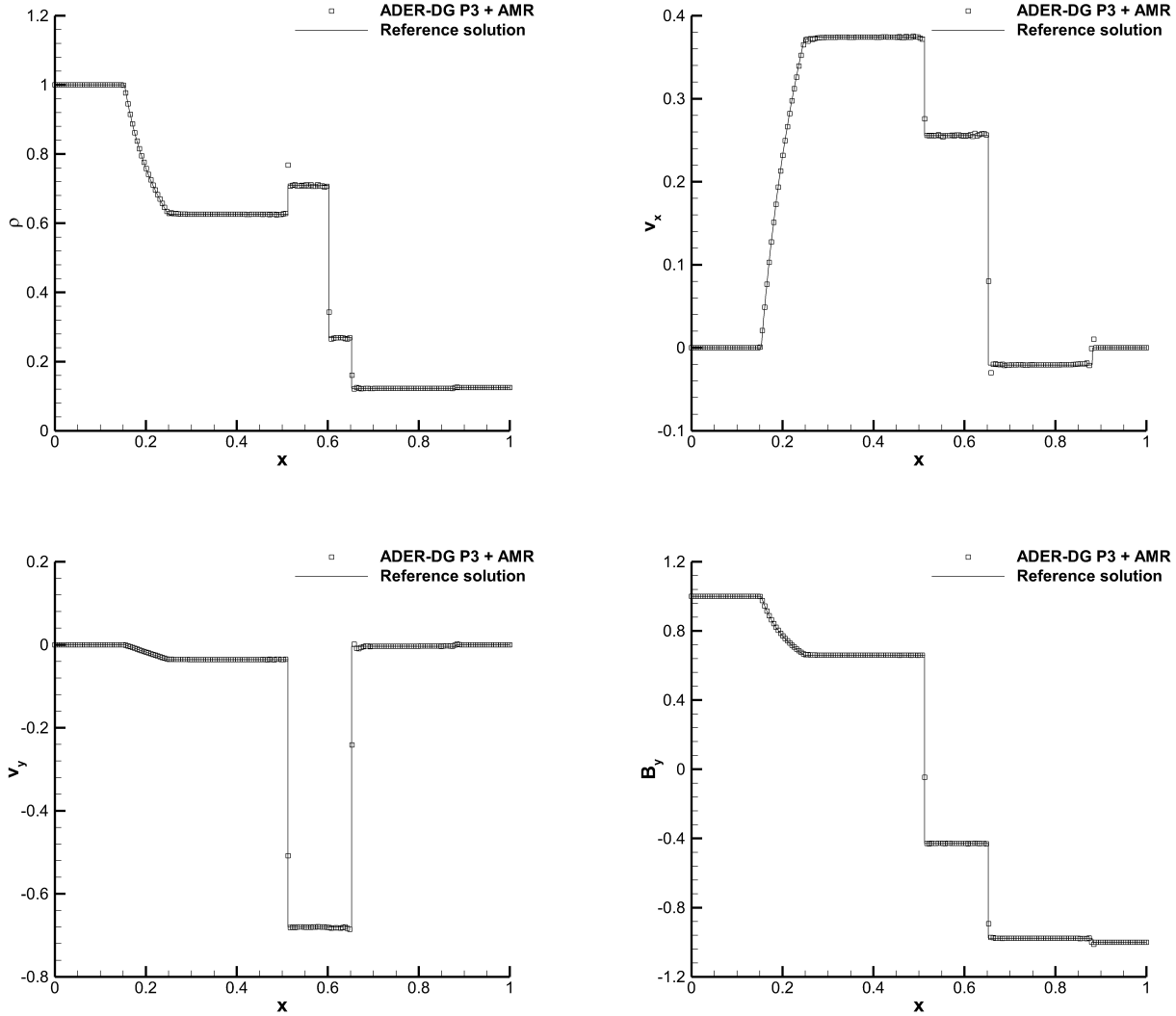


Figure 2. RP1: physical variables interpolated along a 1D cut on 200 equidistant points at $t_{\text{final}} = 0.4$, starting from a coarsest grid of 40×5 elements by using the ADER-DG- \mathbb{P}_3 scheme supplemented with the *a posteriori* ADER-WENO3 subcell limiter.

(1993) and classified as Test 1 and Test 5 in Table 1 of Balsara (2001a). The corresponding initial conditions, referred to as RP1 and RP2 in the following, are given in Tab. 2, which reports also the final times and the adiabatic indices.⁴

The two chosen Riemann problems are solved along two coarse grids of 40×5 and 25×5 elements, respectively. Then, the initial grid is adaptively refined in space and time according to $\tau = 3$ and $\ell_{\text{max}} = 2$. The computational domain is only formally two-dimensional, since the second direction y acts as a passive one. Both tests have been solved using the ADER-DG- \mathbb{P}_3 scheme, supplemented with our *a posteriori* third order ADER-WENO finite volume subcell limiter. The HLL solver has been used for both RP1 and RP2 with a Courant factor $\text{CFL} = 0.5$. The damping factor for the divergence-cleaning procedure is set to $\kappa = 10$.

Figure 1 shows the three-dimensional plot of the solution for the rest mass density and the corresponding AMR grid, by plotting the real DG polynomials (highlighted in blue) for every single unlimited cell and the piecewise linear interpolation of the ADER-WENO limiter along the subcell averages (highlighted in red) for the limited cells. A reference solution for these Riemann problems is computed with the exact Riemann solver proposed by Giacomazzo & Rezzolla (2006). Figures 2 and 3 show the comparison with the reference solution by plotting the rest mass density, the x - and the y - velocity components and the y - component of the magnetic field, interpolated over a one-dimensional cut composed of 200 equidistant points at

⁴ The adiabatic index γ of RP1 is unphysical, as it violates Taub’s inequality based on kinetic theory (Taub 1948; Mignone & McKinney 2007) but it is fixed equal to 2 anyway to ease comparison with vanPutten (1993) and Balsara (2001a).

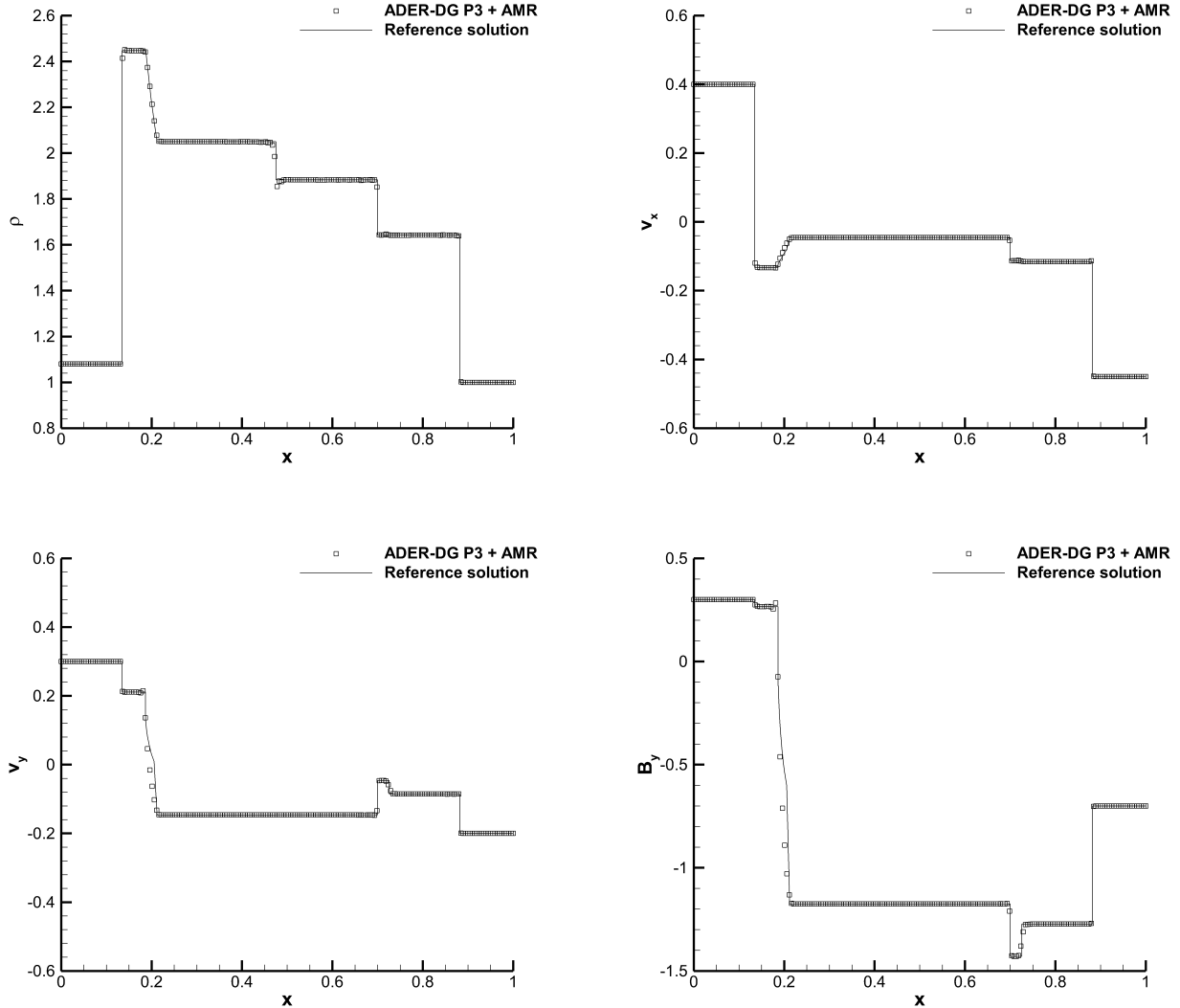


Figure 3. RP2: physical variables interpolated along a 1D cut on 200 equidistant points at $t_{\text{final}} = 0.55$, starting from a coarsest grid of 25×5 elements by using the ADER-DG- \mathbb{P}_3 scheme supplemented with the *a posteriori* ADER-WENO3 subcell limiter.

the final state. A remarkable agreement between the numerical and the reference solution is obtained. All the waves are well captured, five for RP1 and seven for RP2. More specifically, RP1 has a left-going and a right-going fast rarefaction wave, a left-going compound wave, a central contact discontinuity, and a right-going slow shock. RP2 has instead a left-going and a right-going fast shock, a left-going and a right going Alfvén wave, a left-going rarefaction wave, a central contact discontinuity and a right-going slow shock. Due to the combined action of the subcell-limiter and of AMR, all discontinuities are resolved within just one cell or two cells at most. We note that, while the compound wave is absent by construction in the exact solution, its width in the numerical solution is rather small and its amplitude is also comparatively smaller with respect to that obtained with other numerical schemes, like, for instance, in Del Zanna et al. (2007), indicating that this might really be a numerical artifact. However, see also the discussion in Mignone et al. (2009).

The small asymmetries visible in Fig. 1 for RP1 along the passive y direction are attributable to the joint interaction between: (1) the lack of reconstruction in characteristic variables, which could typically help in these cases; (2) some residual *post-shock* oscillations, that in (Balsara 1998) were suppressed by means of artificial viscosity. In spite of these small defects, these results show the capabilities of the new scheme, which does not resort to any artificial viscosity, in resolving the strongly non-linear waves of RMHD equations, for which an unlimited DG schemes would catastrophically fail.

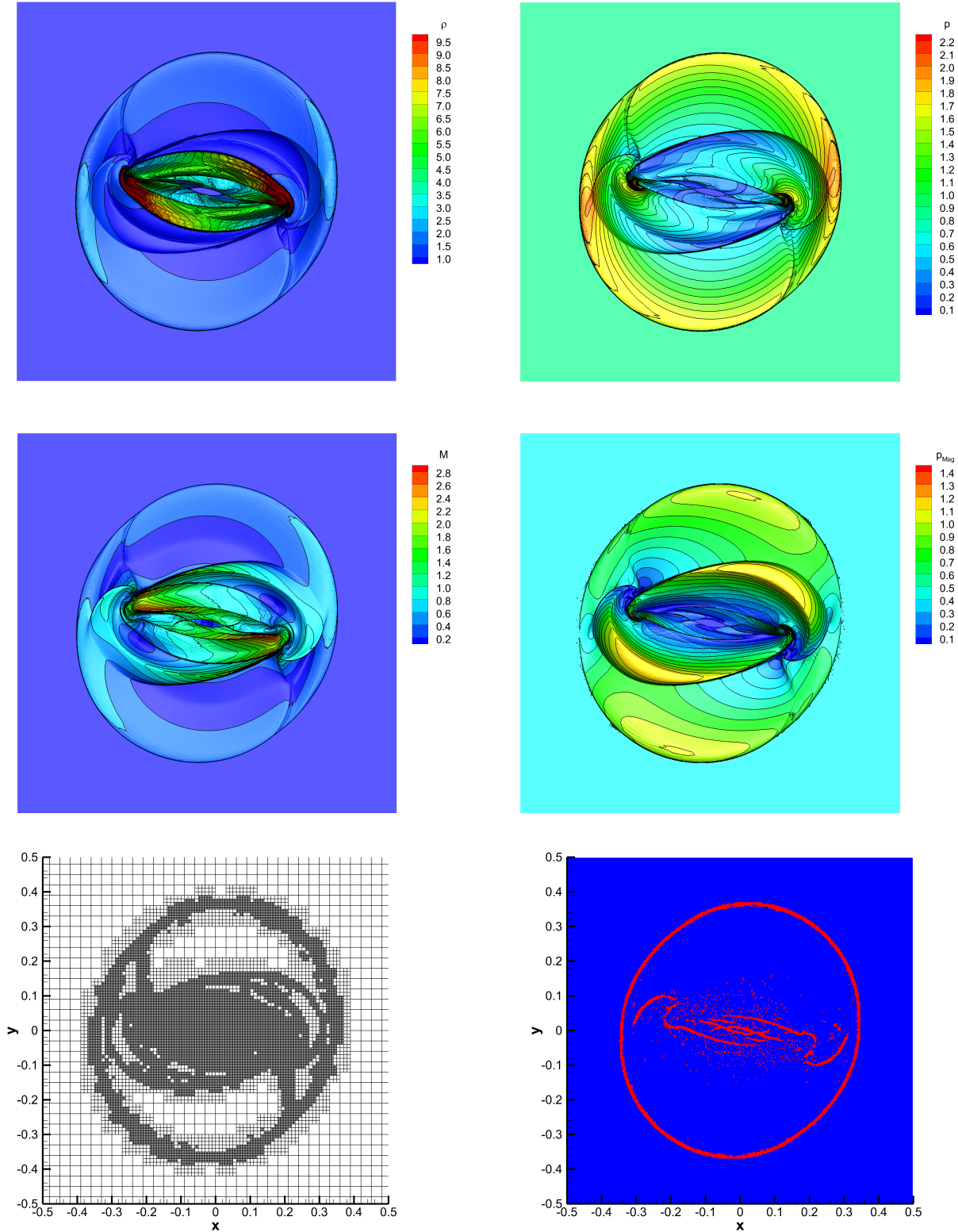


Figure 4. Solution of the RMHD rotor problem at time $t = 0.4$, obtained with the ADER-DG \mathbb{P}_5 scheme supplemented with the *a posteriori* third order ADER-WENO subcell limiter. Top panels: rest-mass density (left) and thermal pressure (right). Central panels: Mach number (left) and magnetic pressure (right). Bottom panels: AMR grid (left) and limiter map (right) with troubled cells marked in red and regular unlimited cells marked in blue.

4.3 The rotor problem

As a first genuinely two dimensional test we consider the relativistic version of the MHD rotor problem, originally proposed by Balsara & Spicer (1999), and solved by a number of authors over the years, including Del Zanna et al. (2003), Dumbser & Zanotti (2009) and Loubère et al. (2014). The computational domain is chosen to be $\Omega = [-0.6, 0.6] \times [-0.6, 0.6]$, discretized on a coarse initial grid formed by 40×40 elements. The AMR framework is activated with a refinement factor $\tau = 3$ and a number of refinement levels $\ell_{\max} = 2$. In this problem a cylinder of a high density fluid is rotating rapidly with angular velocity ω , surrounded by a low density fluid at rest. The initial conditions are in fact given by

$$\rho = \begin{cases} 10 & \text{for } 0 \leq r \leq 0.1; \\ 1 & \text{otherwise;} \end{cases}, \quad \omega = \begin{cases} 8.5 & \text{for } 0 \leq r \leq 0.1; \\ 0 & \text{otherwise;} \end{cases}, \quad \mathbf{B} = \begin{pmatrix} 1.0 \\ 0 \\ 0 \end{pmatrix}, \quad p = 1. \quad (36)$$

Transmissive boundary conditions are applied at the borders. The spinning of the rotor produces torsional Alfvén waves that are launched outside the cylinder, transferring amounts of its initial angular momentum into the external medium. The simulation is performed without any linear taper, that means the physical variables between the internal rotor and the fluid at rest are really discontinuous. The adiabatic index is $\gamma = 4/3$. For this test, the \mathbb{P}_5 version of our ADER-DG scheme was used, combined with the Rusanov Riemann solver.

Fig. 4 shows the rest-mass density, the thermal pressure, the relativistic Mach number M and the magnetic pressure p_{Mag} at time $t = 0.4$. The latter are computed according to

$$M = \frac{Wv}{W_s v_s}, \quad p_{\text{Mag}} = \frac{1}{2} b^2 = \frac{B^2/W + (\mathbf{v} \cdot \mathbf{B})^2}{2}, \quad (37)$$

where v_s is the speed of sound and $W_s = (1 - v_s^2)^{-1/2}$ is the corresponding Lorentz factor. Although an analytic solution is not available for this test, the results shown are in very good qualitative agreement with those already reported in the literature. Moreover, the adopted divergence-cleaning approach works accurately as expected, with no appreciable spurious oscillations generated in the rest mass density or in the magnetic field. Lastly, the behaviour of the space-time AMR and of the *a posteriori* limiter is depicted in the two bottom panels of Fig. 4: the final mesh is shown in the left panel, whereas in the right the troubled zones are represented in red. Clearly, the activation of the limiter becomes necessary only in a limited number of cells, and precisely where discontinuities are stronger.

4.4 Orszag-Tang vortex system

As a second two dimensional academic test we have chosen the relativistic version of the well known Orszag-Tang vortex problem, proposed by Orszag & Tang (1979), and later considered by Picone & Dahlburg (1991) and Dahlburg & Picone (1989). The resistive case of this relativistic MHD problem has been investigated by Dumbser & Zanotti (2009). The initial conditions are given by

$$(\rho, u, v, w, p, B_x, B_y, B_z) = \left(1, -\frac{3}{4\sqrt{2}} \sin(y), \frac{3}{4\sqrt{2}} \sin(x), 0, 1, -\sin(y), \sin(2x), 0 \right), \quad (38)$$

while the adiabatic index is $\gamma = 4/3$. The equations are discretized over the computational domain $\Omega = [0, 2\pi] \times [0, 2\pi]$, with 30×30 elements on the coarsest refinement level at the initial state. Periodic boundary conditions are imposed at the borders and the Rusanov Riemann solver is adopted. The relevant AMR parameters are $\tau = 3$ and $\ell_{\max} = 2$. We note that the maximally refined AMR mesh corresponds to a uniform grid formed of $270 \times 270 = 72,900$ elements. Moreover, the \mathbb{P}_5 version of the ADER-DG scheme that we have adopted uses 6 degrees of freedom per spatial dimension, amounting to a total resolution of 2,624,400 spatial degrees of freedom. The computed solution for the rest-mass density is shown in the central column of Fig. 5, at times $t = 0.5, 2.0, 3.0, 4.0$ respectively. For comparison, the panels on the right column show the results of a simulation performed over the maximally refined uniform mesh, which can be used as a reference solution. Clearly, an excellent agreement between the AMR results and this reference solution is obtained. As before, this test confirms the ability of the proposed method for solving complex two dimensional problems and, by showing the critical cells which required the activation of the limiter, it provides an immediate visual sketch of the most delicate regions over the computational domain.

5 THE RMHD KELVIN-HELMHOLTZ INSTABILITY

A two-dimensional test that is not only academic but may be relevant to explain the observed phenomenology of extended radio-jets [see Martí & Müller (2003) and references therein], we consider the Kelvin-Helmholtz (KH) instability with an initially uniform magnetic field. Following the works of Mignone et al. (2009), Beckwith & Stone (2011) and Radice &

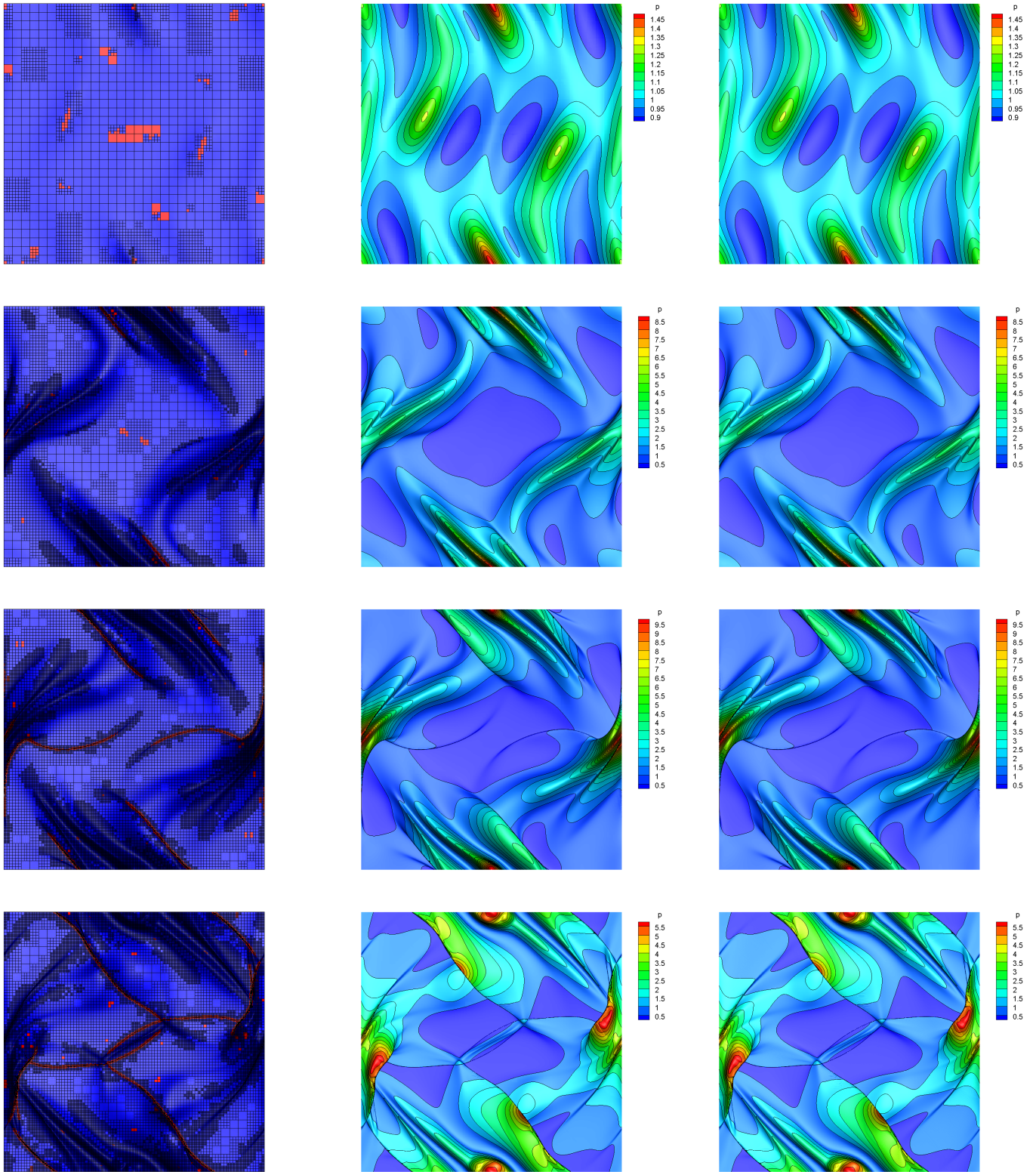


Figure 5. RMHD Orszag-Tang vortex problem at times $t = 0.5$, $t = 2.0$, $t = 3.0$, $t = 4.0$, from top to bottom, obtained through the ADER-DG- \mathbb{P}_5 scheme supplemented with the third order *a posteriori* ADER-WENO subcell limiter. Left panels: AMR-grid, troubled cells (red) and unlimited cells (blue). Central panels: \mathbb{P}_5 -solution obtained on the AMR grid. Right panels: \mathbb{P}_5 -solution obtained on the fine uniform grid corresponding to the finest AMR grid level.

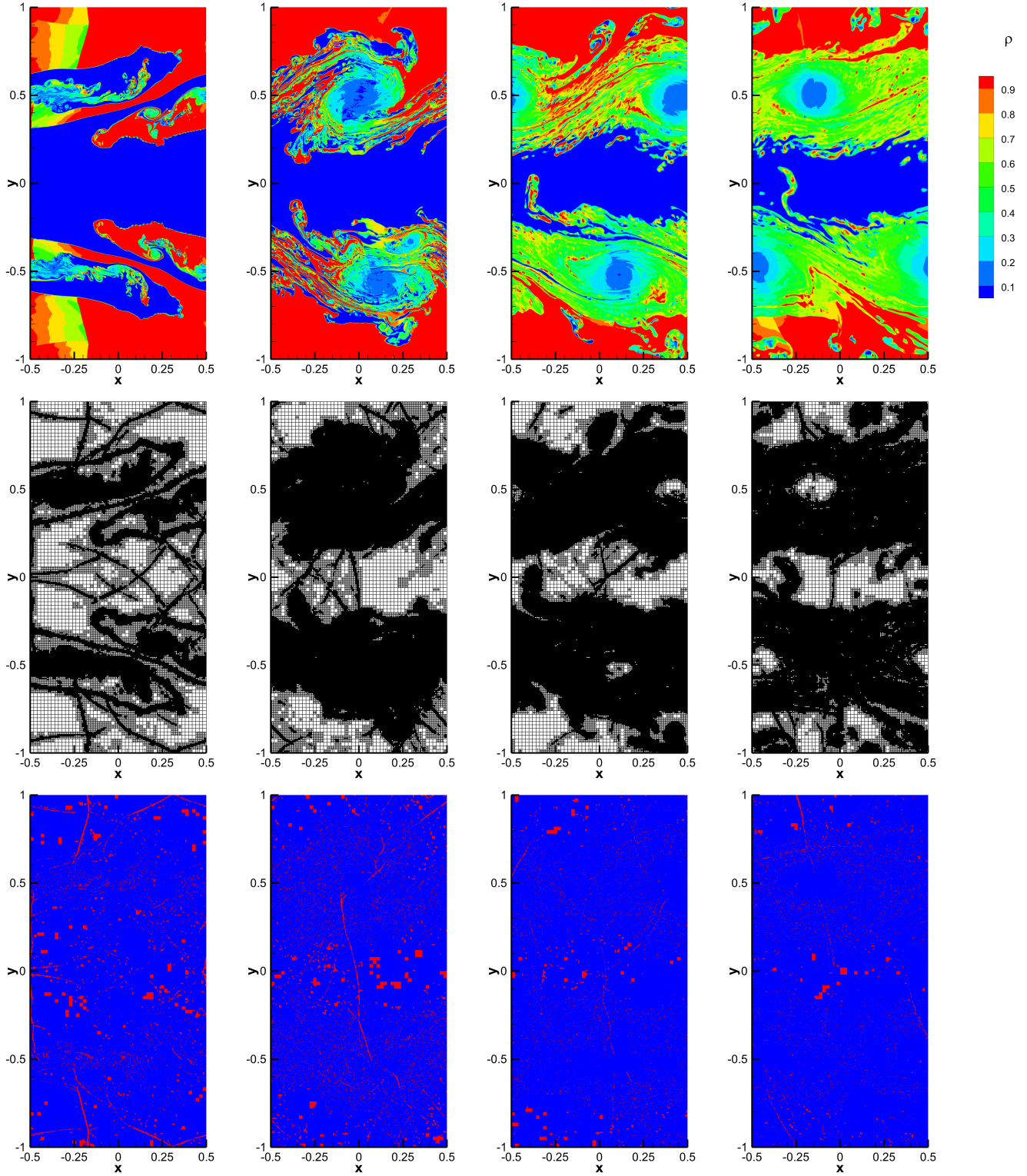


Figure 6. RMHD Kelvin-Helmholtz instability at times $t = 5.0$, $t = 10.0$, $t = 20.0$, $t = 30.0$ from left to right, obtained through the ADER-DG- \mathbb{P}_3 scheme supplemented with the second order *a posteriori* ADER-TVD subcell limiter. The computed solution of density (top), AMR grid (center) and limiter map (bottom) are shown.

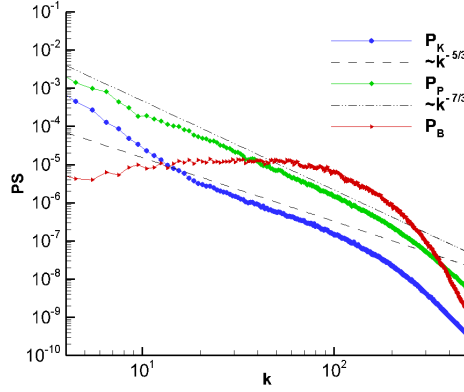


Figure 7. Power spectra for the RMHD Kelvin-Helmholtz instability at time $t = 30.0$ obtained through the ADER-DG- \mathbb{P}_3 scheme.

Rezzolla (2012), we choose the initial conditions as

$$v_x = \begin{cases} v_s \tanh [(y - 0.5)/a] & y > 0, \\ -v_s \tanh [(y + 0.5)/a] & y \leq 0, \end{cases} \quad (39)$$

where $v_s = 0.5$ is the velocity of the shear layer and $a = 0.01$ is its characteristic size. Although not necessary in principle, it is convenient to introduce a small transverse velocity to trigger the instability, hence fixing

$$v_y = \begin{cases} \eta_0 v_s \sin(2\pi x) \exp[-(y - 0.5)^2/\sigma] & y > 0, \\ -\eta_0 v_s \sin(2\pi x) \exp[-(y + 0.5)^2/\sigma] & y \leq 0, \end{cases} \quad (40)$$

where $\eta_0 = 0.1$ and $\sigma = 0.1$. Finally, the rest-mass density is chosen as

$$\rho = \begin{cases} \rho_0 + \rho_1 \tanh [(y - 0.5)/a] & y > 0, \\ \rho_0 - \rho_1 \tanh [(y + 0.5)/a] & y \leq 0, \end{cases} \quad (41)$$

with $\rho_0 = 0.505$ and $\rho_1 = 0.495$. The adiabatic index is $\gamma = 4/3$, the pressure is $p = 1$ everywhere, and we add a weak uniform magnetic field along the x - direction, namely $B_x = 0.001$. The simulations are run with the ADER-DG- \mathbb{P}_3 scheme over the computational domain $\Omega = [-0.5, 0.5] \times [-1, 1]$, using 50×100 elements on the coarsest refinement level at the initial state. Periodic boundary conditions are imposed along all borders and the Rusanov Riemann solver is adopted. AMR is activated with $\tau = 3$ and $\ell_{\max} = 2$. In this simulation the solution on the subgrid has been evolved through a second order TVD scheme, which turned out to be more robust than the usual third order WENO method. Fig. 6 shows the rest-mass density field at various times, up to $t = 30$, and the corresponding development of the KH instability. Since no physical viscosity or resistivity is present, it is very difficult to judge about the physical nature of the tiny structures, especially secondary instabilities, which are produced during the evolution, and which have been shown to depend sensibly on the order of accuracy of the scheme and on the Riemann solver used (Beckwith & Stone 2011; Radice & Rezzolla 2012; Zanotti & Dumbser 2015). As the instability proceeds, the transition to a turbulent state occurs. Although our final time is not large enough to allow for a fully developed turbulent state, and although this paper is not devoted to a detailed study of relativistic MHD turbulence (see instead the works by Zhang et al. (2009); Zrake & MacFadyen (2012); Garrison & Nguyen (2015)), we have nevertheless computed the power spectra of a few relevant quantities to confirm that the transition to turbulence is indeed taking place. Fig. 7, in particular, shows the power spectra of the velocity field, of the pressure field and of the magnetic field, which have been computed according to

$$P_v(k) = \frac{1}{2} \int_{|\mathbf{k}|=k} |\hat{v}(\mathbf{k})|^2 d\mathbf{k}, \quad P_p(k) = \int_{|\mathbf{k}|=k} |\hat{p}(\mathbf{k})|^2 d\mathbf{k}, \quad P_B(k) = \int_{|\mathbf{k}|=k} |\hat{B}(\mathbf{k})|^2 d\mathbf{k}, \quad (42)$$

where \mathbf{k} is the wave-number, while $\hat{v}(\mathbf{k})$, $\hat{B}(\mathbf{k})$, $\hat{p}(\mathbf{k})$ are the two-dimensional Fourier-transforms of \mathbf{v} , p and \mathbf{B} , respectively. For $k \approx [20, 70]$, in the so-called *inertial range* where the dynamics of the turbulence is not affected by large scale energy inputs nor by dissipation, we approximately recover Kolmogorov's trends, namely $P_v(k) \propto k^{-5/3}$ and $P_p(k) \propto k^{-7/3}$ (Biskamp 2008). The power spectrum of the magnetic field is instead in qualitative agreement with results obtained by Zhang et al. (2009) for fully turbulent configurations. A dedicated analysis to astrophysical RMHD turbulence will be presented in a separate work.

6 DISCUSSION AND CONCLUSIONS

We have proposed a novel approach for the numerical solution of the special relativistic magnetohydrodynamics equations, which is based on the discontinuous Galerkin finite element method, but with some crucial modifications. Pure DG schemes, in fact, cannot avoid the appearance of oscillations when discontinuities form in the solution. The common practice in these cases is to resort to either artificial viscosity, filtering, or to an *a priori* finite-volume-type limiting of the higher order moments of the DG scheme, thus spoiling the subcell resolution capabilities of the DG scheme. On the contrary, following the recent works by Dumbser et al. (2014) and Zanotti et al. (2014), it is possible to verify *a posteriori* the validity of the candidate solution provided by the pure DG scheme by applying a relaxed form of the discrete maximum principle and by checking the numerical solution for physical validity, i.e. for positivity, subluminal velocities and for possible failures in the conversion from the conservative to the primitive variables. For those cells that violate any of the two criteria, we scatter the DG polynomials, computed at the previous (safe) time step, onto a set of $N_s = 2N + 1$ subcells along each spatial direction. After that, a traditional and more robust WENO finite volume scheme, or an even more robust TVD scheme, is applied at the *subcell level*, thus *recomputing* the solution in the troubled cells. In this way, our special *a posteriori* subcell limiter of the DG method is intrinsically based on the governing partial differential equations, while standard DG limiters act independently of the governing PDE. The new, and thereby safe, subcell averages are subsequently gathered back into high order cell-centered DG polynomials on the main grid through a subgrid reconstruction operator. The *a posteriori* limiter that we have used can also be regarded as a discontinuity detector. This is clear, for instance, after looking at the bottom right panel of Fig. 4, or at the left panels of the Fig. 5, where the activation of the limiter occurs where strong discontinuities are present. In this respect, our *a posteriori* correction may resemble the logic behind *a priori* limiters based on *shock detectors*, several forms of which have been introduced, both in the Newtonian and in the relativistic framework. However, the *a posteriori* approach that we have developed has at least two evident advantages over traditional *shock detectors*. The first one is that it is both very simple and it applies unmodified for general systems of equations, while shock detectors become more and more elaborate as the complexity of the equations increases.⁵ The second advantage is that the *a posteriori* approach can capture all kind of discontinuous solutions, including contact discontinuities, which are invisible to shock detectors but often represent a serious challenge to the numerical scheme.

We also stress that both the DG scheme on the main grid and the WENO finite volume scheme on the subgrid are implemented with the local spacetime discontinuous Galerkin predictor of Dumbser et al. (2008), thus providing a high order one-step ADER scheme in time, with no need for the Runge–Kutta time discretization that is typically used in the so-called method of lines. Finally, adaptive mesh refinement (AMR) is used, implying that the two AMR operations of projection and averaging need to involve the subcell averages of the solution on the sub-grids.

The new ADER-DG-AMR scheme, which has been validated over stringent academic tests, can contribute significantly to the numerical modeling of high energy astrophysics systems, such as extragalactic jets, gamma-ray bursts and magnetospheres of neutron stars. Work is already in progress to extend this approach to the full general relativistic regime. A particularly attracting field of application for the new method is represented by the study of relativistic turbulence, that we have considered here in a simplified and preliminary two-dimensional set up in which the transition to turbulence is induced by the Kelvin–Helmholtz instability. We plan to investigate this problem in the future by means of three-dimensional simulations in which the high order capabilities of DG schemes are fully exploited.

ACKNOWLEDGMENTS

The research presented in this paper was financed by the European Research Council (ERC) under the European Union’s Seventh Framework Programme (FP7/2007-2013) with the research project *STiMulUs*, ERC Grant agreement no. 278267.

The authors are also very grateful for the subsequent financial support of the present research, already granted by the European Commission under the H2020-FETHPC-2014 programme with the research project *ExaHyPE*, grant agreement no. 671698.

We are grateful to Bruno Giacomazzo and Luciano Rezzolla for providing the numerical code for the exact solution of the Riemann problem in RMHD. We would also like to acknowledge PRACE for awarding access to the SuperMUC supercomputer based in Munich, Germany at the Leibniz Rechenzentrum (LRZ).

REFERENCES

- Anderson M., Hirschmann E., Liebling S. L., Neilsen D., 2006, *Classical Quantum Gravity*, 23, 6503
- Anile A. M., 1990, *Relativistic Fluids and Magneto-fluids*. Cambridge University Press

⁵ See Zanotti et al. (2010) for a shock detector valid in general relativistic hydrodynamics.

- Antón L., Miralles J. A., Martí J. M., Ibáñez J. M., Aloy M. A., Mimica P., 2010, *Astrophys. J. Suppl.*, 188, 1
- Antón L., Zanotti O., Miralles J. A., Martí J. M., Ibáñez J. M., Font J. A., Pons J. A., 2006, *Astrophys. J.*, 637, 296
- Balsara D., 1998, *Astrophysical Journal Suppl. Series*, 116, 133
- Balsara D., 2001a, *Astrophysical Journal Suppl. Series*, 132, 83
- Balsara D., Meyer C., Dumbser M., Du H., Xu Z., 2013, *Journal of Computational Physics*, 235, 934
- Balsara D., Spicer D., 1999, *Journal of Computational Physics*, 149, 270
- Balsara D. S., 2001b, *Journal of Computational Physics*, 174, 614
- Balsara D. S., Altmann C., Munz C., Dumbser M., 2007, *Journal of Computational Physics*, 226, 586
- Barkov M., Komissarov S. S., Korolev V., Zankovich A., 2014, *Mon. Not. R. Astron. Soc.*, 438, 704
- Barth T., Frederickson P., 1990, *AIAA paper no. 90-0013*
- Baumgarte T. W., Shapiro S. L., 2003, *Astrophys. Journal*, 585, 921
- Beckwith K., Stone J. M., 2011, *The Astrophysical Journal Supplement Series*, 193, 6
- Begelman M. C., Blandford R. D., Rees M. J., 1984, *Reviews of Modern Physics*, 56, 255
- Biskamp D., 2008, *Magnetohydrodynamic Turbulence*
- Bucciantini N., Del Zanna L., 2013, *Mon. Not. R. Astron. Soc.*, 428, 71
- Casoni E., Peraire J., Huerta A., 2013, *International Journal for Numerical Methods in Fluids*, 71, 737
- Cesenek J., Feistauer M., Horacek J., Kucera V., Prokopova J., 2013, *Applied Mathematics and Computation*, 219, 7139
- Clain S., Diot S., Loubère R., 2011, *Journal of Computational Physics*, 230, 4028
- Cockburn B., Hou S., Shu C. W., 1990, *Mathematics of Computation*, 54, 545
- Cockburn B., Lin S. Y., Shu C., 1989, *Journal of Computational Physics*, 84, 90
- Cockburn B., Shu C. W., 1989, *Mathematics of Computation*, 52, 411
- Cockburn B., Shu C. W., 1991, *Mathematical Modelling and Numerical Analysis*, 25, 337
- Cockburn B., Shu C. W., 1998, *Journal of Computational Physics*, 141, 199
- Dahlburg R. B., Picone J. M., 1989, *Phys. Fluids B*, 1, 2153
- Dedner A., Kemm F., Kröner D., Munz C.-D., Schnitzer T., Wesenberg M., 2002, *Journal of Computational Physics*, 175, 645
- Del Zanna L., Bucciantini N., Londrillo P., 2003, *Astron. Astrophys.*, 400, 397
- Del Zanna L., Zanotti O., Bucciantini N., Londrillo P., 2007, *Astron. Astrophys.*, 473, 11
- Dionysopoulou K., Alic D., Palenzuela C., Rezzolla L., Giacomazzo B., 2013, *Phys. Rev. D*, 88, 044020
- Diot S., Clain S., Loubère R., 2012, *Computers and Fluids*, 64, 43
- Duez M. D., Liu Y. T., Shapiro S. L., Stephens B. C., 2005, *Phys. Rev. D*, 72, 024028
- Dumbser M., Balsara D. S., Toro E. F., Munz C.-D., 2008, *Journal of Computational Physics*, 227, 8209
- Dumbser M., Enaux C., Toro E., 2008, *Journal of Computational Physics*, 227, 3971
- Dumbser M., Kaeser M., Titarev V. A., Toro E. F., 2007, *Journal of Computational Physics*, 226, 204
- Dumbser M., Munz C., 2006, *Journal of Scientific Computing*, 27, 215
- Dumbser M., Uuriintsetseg A., Zanotti O., 2012, *ArXiv e-prints*
- Dumbser M., Zanotti O., 2009, *Journal of Computational Physics*, 228, 6991
- Dumbser M., Zanotti O., Hidalgo A., Balsara D. S., 2013, *Journal of Computational Physics*, 248, 257
- Dumbser M., Zanotti O., Loubère R., Diot S., 2014, *Journal of Computational Physics*, 278, 47
- Etienne Z. B., Liu Y. T., Shapiro S. L., 2010, *Phys. Rev. D*, 82, 084031
- Fechter S., Munz C.-D., 2015, *International Journal for Numerical Methods in Fluids*, pp n/a–n/a
- Garrison D., Nguyen P., 2015, *ArXiv e-prints*
- Giacomazzo B., Rezzolla L., 2006, *Journal of Fluid Mechanics*, 562, 223
- Giacomazzo B., Rezzolla L., 2007, *Classical Quantum Gravity*, 24, S235
- Hidalgo A., Dumbser M., 2011, *Journal of Scientific Computing*, 48, 173
- H.Luo J.D.Baum R.Löhner 2007, *J. Comput. Phys.*, 225, 686
- Honkkila V., Janhunen P., 2007, *Journal of Computational Physics*, 223, 643
- H.Zhu J.Qiu 2013, *Advances in Computational Mathematics*, 39, 445
- J.Qiu C-W.Shu 2004, *J. Comput. Phys.*, 193, 115
- J.Zhu Qiu J., C-W.Shu M.Dumbser 2008, *J. Comput. Phys.*, 227, 4330
- J.Zhu X.Zhong C. S., Qiu J., 2013, *J. Comp. Phys.*, 248, 200
- Keppens R., Meliani Z., van Marle A. J., Delmont P., Vlasis A., van der Holst B., 2012, *Journal of Computational Physics*, 231, 718
- Khokhlov A., 1998, *Journal of Computational Physics*, 143, 519
- Kim J., Balsara D. S., 2014, *Journal of Computational Physics*, 270, 634
- Komissarov S. S., 1997, *Physics Letters A*, 232, 435
- Komissarov S. S., 1999, *Mon. Not. R. Astron. Soc.*, 303, 343

- Komissarov S. S., 2007, *Mon. Not. R. Astron. Soc.*, 382, 995
- Kouveliotou C., Meegan C. A., Fishman G. J., Bhat N. P., Briggs M. S., Koshut T. M., Paciesas W. S., Pendleton G. N., 1993, *Astrophys. J.*, 413, L101
- Krivodonova L., R.Qin 2013, *Applied Numerical Mathematics*, 64, 1
- Lax P. D., Wendroff B., 1960, *Commun. Pure Appl. Math.*, 13, 217
- Lhner R., 1987, *Computer Methods in Applied Mechanics and Engineering*, 61, 323
- Liu Y., Vinokur M., Wang Z., 2006, *Journal of Computational Physics*, 212, 454
- L.Krivodonova 2007, *Journal of Computational Physics*, 226, 879
- Londrillo P., Del Zanna L., 2000, *Astrophysical Journal*, 530, 508
- Loubère R., Dumbser M., Diot S., 2014, *Communication in Computational Physics*, 16, 718
- Martí J. M., Müller E., 2003, *Living Rev. Relativ.*, 6, 7; <http://www.livingreviews.org/lrr>
- Michel F. C., 1991, *Theory of neutron star magnetospheres*
- Mignone A., Bodo G., 2006, *Mon. Not. R. Astron. Soc.*, 368, 1040
- Mignone A., McKinney J. C., 2007, *Mon. Not. R. Astron. Soc.*, 378, 1118
- Mignone A., Ugliano M., Bodo G., 2009, *Monthly Notices of the Royal Astronomical Society*, 393, 1141
- Mignone A., Zanni C., Tzeferacos P., van Straalen B., Colella P., Bodo G., 2012, *Astrophys. J. Suppl. Ser.*, 198, 7
- Neilsen D., Hirschmann E. W., Millward R. S., 2006, *Classical and Quantum Gravity*, 23, 505
- Noble S. C., Gammie C. F., McKinney J. C., Del Zanna L., 2006, *Astrophys. J.*, 641, 626
- Orszag S. A., Tang C. M., 1979, *Journal of Fluid Mechanics*, 90, 129
- Palenzuela C., Lehner L., Reula O., Rezzolla L., 2009, *Mon. Not. R. Astron. Soc.*, 394, 1727
- Persson P.-O., Peraire J., 2006, *AIAA Paper 2006-112*
- Picone J. M., Dahlburg R. B., 1991, *Phys. Fluids B*, 3, 29
- Qiu J., Dumbser M., Shu C., 2005, *Computer Methods in Applied Mechanics and Engineering*, 194, 4528
- Qiu J., Shu C., 2005, *SIAM Journal on Scientific Computing*, 26, 907
- Radice D., Rezzolla L., 2011, *Phys. Rev. D*, 84, 024010
- Radice D., Rezzolla L., 2012, *Astron. Astrophys.*, 547, A26
- R.Hartmann P.Houston 2002, *J. Comp. Phys.*, 183, 508
- Solin P., 2006, *Partial Differential Equations And the Finite Element Method. Pure and Applied Mathematics*, Wiley-Interscience
- Sonntag M., Munz C., 2014, in Fuhrmann J., Ohlberger M., Rohde C., eds, *Finite Volumes for Complex Applications VII Shock capturing for discontinuous galerkin methods using finite volume subcells*. Springer, pp 945–953
- Takamoto M., Inoue T., 2011, *Astrophys. J.*, 735, 113
- Taub A. H., 1948, *Phys. Rev.*, 74, 328
- Titarev V., Toro E., 2002, *Journal of Scientific Computing*, 17, 609
- Titarev V., Toro E., 2005, *Journal of Computational Physics*, 204, 715
- Titarev V. A., Toro E. F., 2004, *Journal of Computational Physics*, 201, 238
- Toro E., 1999, *Riemann Solvers and Numerical Methods for Fluid Dynamics*, second edn. Springer
- Toro E. F., Titarev V. A., 2002, *Proceedings of the Royal Society of London. Series A: Mathematical, Physical and Engineering Sciences*, 458, 271
- Toth G., 2000, *Journal of Computational Physics*, 161, 605
- vanPutten M. H., 1993, *Journal of Computational Physics*, 105, 339
- Wang Z., Zhang L., Liu Y., 2004, *Journal of Computational Physics*, 194, 716
- Zanotti O., Dumbser M., 2011, *Mon. Not. R. Astron. Soc.*, 418, 1004
- Zanotti O., Dumbser M., 2015, *Computer Physics Communications*, 188, 110
- Zanotti O., Fambri F., Dumbser M., Hidalgo A., 2014, *ArXiv e-prints*
- Zanotti O., Rezzolla L., Del Zanna L., Palenzuela C., 2010, *Astron. Astrophys.*, 523, A8+
- Zanotti O., Roedig C., Rezzolla L., Del Zanna L., 2011, *Mon. Not. R. Astron. Soc.*, 417, 2899
- Zenitani S., Hesse M., Klimas A., 2009, *Astrophys. J.*, 696, 1385
- Zenitani S., Hesse M., Klimas A., 2010, *Astrophysical Journal Lett.*, 716, L214
- Zhang W., MacFadyen A., Wang P., 2009, *Astrophys. J.*, 692, L40
- Zrake J., MacFadyen A. I., 2012, *Astrophys. J.*, 744, 32
- Zumbusch G., 2009, *Classical Quantum Gravity*, 26, 175011